Wetting and drainage cycles in two New Zealand soil types: Effects on relative gas diffusivity and N2O emissions

Camille Rousset, Timothy Clough, Peter Grace, David Rowlings, Clemens Scheer

Title: Wetting and drainage cycles in two New Zealand soil types: effects on relative gas diffusivity and N_2O emissions.

Authors: Camille Rousset[A,D], Timothy J. Clough[A], Peter R. Grace[B], David W. Rowlings[B], Clemens Scheer[B,C].

Author address:

[A] Department of Soil and Physical Sciences, Lincoln University, PO Box 85084, Lincoln, 7647, New Zealand

[B] Queensland University of Technology, Institute for Future Environment, 2 George Street, Brisbane, Queensland, 4000, Australia

[C] Institut für Meteorologie und Klimaforschung, Department Atmosphärische Umweltforschung (IMK-IFU), KIT-Campus Alpin, Garmisch-Partenkirchen, Germany.

[D] Agroécologie, AgroSup Dijon, INRAE, Univ. Bourgogne Franche-Comté, Dijon, France

Corresponding author:

Camille Rousset : Camille.Rousset@lincolnuni.ac.nz

Highlights:

- Nitrous oxide emissions are highest when D_p/D_o indicates anaerobic conditions
- Soil wetting-drainage cycle effects on D_p/D_o and N_2O emissions depend on soil
- Intra-aggregate pores implicated as N_2O emission site during well-structured soil drainage
- High organic matter may alter O_2 demand and D_p/D_o - N_2O relationships

Abstract

Nitrous oxide (N_2O) is a potent greenhouse gas generated in agricultural soils by microbial processes that vary according to soil redox. Soil oxygen (O_2) supply and demand strongly influence soil redox. Migration of O_2 into the soil primarily occurs via gas diffusion, expressed as relative gas diffusivity (D_p/D_o), and is influenced by soil structure (air-filled porosity and tortuosity of pores) and soil water content. Soil N_2O emissions have been shown to increase at low values of D_p/D_o but detailed studies examining the relationship between D_p/D_o and soil N_2O emissions remain limited, with relatively few soil types examined, and no studies of repeated wetting-drainage cycles. Thus, the objectives of this study were to examine how successive wetting-drainage cycles affected both D_p/D_o dynamics and associated N_2O emissions in two New Zealand soils; a pallic silt loam and an allophanic loam, with the latter also having a higher organic matter content. Soil cores, repacked to varying density, were wetted up with ^{15}N enriched NO_3^- solution and placed on tension tables where they underwent two consecutive 12-day wetting-drainage cycles from saturation to field capacity (0 to -10 kPa). Over time measurements were made of N_2O, N_2, inorganic-N and soluble carbon, while D_p/D_o was modelled using soil physical characteristics. For both soils each wetting-drainage cycle induced N_2O fluxes but with 5-fold lower fluxes in the allophanic soil. Greater aggregation and sand content in the allophanic soil generated higher porosity and D_p/D_o values that were almost always greater than recognized anaerobic limits. Thus, wetting-induced N_2O fluxes observed in the allophanic soil during early drainage were concluded to result from anaerobic or hypoxic pathways of N_2O production potentially within the intra-aggregate zone. While wetting-drainage events induce N_2O emissions by altering D_p/D_o and the soil aeration status, the draining of soils, especially soils high in organic matter, may enhance O_2 demand generating anaerobic zones conducive to denitrification. Further detailed studies examining the interaction

between soil structure and soil organic matter content and their effect on N_2O emissions under wetting-drainage events, with measures of soil O_2, are needed.

Keywords: ^{15}N, bulk density, denitrification, dinitrogen, matric potential, mineralization, nitrification

Abbreviations: Nitrous Oxide (N_2O), Nitrate (NO_3^-), Dissolved Organic Carbon (DOC), Bulk density (soil ρ_b), Particle density (ρ_d), Matric potential (ψ), Soil-gas diffusivity (D_p/D_o), Water-filled pore space (WFPS), Air-filled pore space (ε), Porosity (Φ).

1. Introduction

Nitrous oxide (N_2O) is a potent greenhouse gas linking reactive N to climate change (Erisman et al., 2011). The N_2O molecule is also the dominant stratospheric ozone depleting substance (Ravishankara et al., 2009). Atmospheric concentrations of N_2O are currently 20% higher than pre-industrial levels (Ciais et al., 2013). Agriculture dominates anthropogenic N_2O emissions, accounting for 4.1 (1.7-4.8) Tg N (N_2O) yr^{-1} out of an estimated 6.9 Tg N (N_2O) yr^{-1} of anthropogenic N_2O emissions (Ciais et al., 2013), as a consequence of fertiliser N and animal excreta deposition (Davidson, 2009).

Fertiliser and manure N, applied to soils, contribute to N_2O emissions as the result of ensuing N transformations, predominately via microbial pathways, that include nitrification, nitrifier-denitrification, and denitrification (Wrage et al., 2001; Wrage-Mönnig et al., 2018; Stein, 2019). The soil O_2 concentration influences the relative dominance of N_2O producing pathways: nitrification, nitrifier-denitrification and denitrification are aerobic, hypoxic, and

anaerobic processes, respectively. Several other microbial pathways, such as DNRA (dissimilatory nitrate reduction to ammonium) can also generate N_2O (Friedl et al., 2018; Wrage-Mönnig et al., 2018) and these are also influenced by soil O_2 concentration and redox status. Soil redox potential is the propensity for electrons to be transferred from reduced forms (electron donors e.g. organic matter) to electron acceptors (e.g. nitrate). Lower and upper redox potential boundaries in soil are governed by the reduction of CO_2 to methane and the presence of O_2, respectively (Reddy and Delaune, 2008). Thus, redox declines as the ability for O_2 to diffuse into the soil (*Dp/Do*) decreases or if O_2 consumption exceeds O_2 supply. If the soil becomes anaerobic alternative electron acceptors such as nitrate replace O_2 (Reddy and Delaune, 2008).

Thus, critical to understanding the role microbes perform in controlling N_2O emissions is a better grasp of how the availability of O_2 within a soil may change. Subsurface movement of gas within a soil occurs primarily via diffusion. Assuming no change in atmospheric pressure or wind-induced disturbance the movement of gas across the soil atmosphere interface is also diffusion controlled. The migration of a gas can be described by a soil gas diffusion coefficient (D_p, cm^3 soil air cm^{-1} s^{-1}) which is a parameter that varies with the characteristics of a gas, soil atmosphere temperature and pressure, soil structure (e.g. air-filled porosity and tortuosity of pores) and soil water content (Rolston and Moldrup, 2012). The diffusion coefficient of the same gas in free air (D_o, cm^2 air s^{-1}) is used to normalise D_p, so that soil-gas diffusivity (D_p/D_o) can be expressed under a given set of conditions (Rolston and Moldrup, 2012).

Since the conceptual work of Linn and Doran (1984), changes in a soil's water-filled pore space (WFPS) have routinely been used to explain variation in N_2O fluxes. However, WFPS, which defines the proportion of total pore space filled with water, is a normalised dimensionless value and Farquharson and Baldock (2007) stated that "…WFPS does not quantify the fraction of the entire soil volume that is filled with water or air and hence is not

directly proportional to the diffusion of gases and solutes that regulate process rates across soils with different total porosities". This was demonstrated by Balaine et al. (2013) who found that peak N_2O emissions, from soil cores treated with nitrate and spanning bulk densities from 1.1 to 1.5 Mg m^{-3}, occurred across a WFPS range of 67-80%. Farquharson and Baldock (2007) went on to suggest that simple measures of soil water content combined with soil structural parameters should be considered, in conjunction with volume fractions of air or water. Thus, Balaine et al. (2013) further assessed N_2O emissions relative to D_p/D_o and found strong relationships between N_2O emissions and D_p/D_o with N_2O emissions peaking at a D_p/D_o value of 0.006 regardless of the soil bulk density. Further assessment of this relationship was undertaken by Balaine et al. (2016) who, using the same soil, found that cumulative N_2O and N_2 emissions, after 35 days, also depended on D_p/D_o. A laboratory study by Petersen et al. (2008) also found D_p/D_o explained N_2O emissions better than WFPS when examining soil across seven matric potentials. Petersen et al. (2013) observed that carbon (C) inputs, resulting from crop system management or freeze-thaw effects could potentially affect the relationship between peak emissions of N_2O and calculated D_p/D_o. Values of $D_p/D_o < 0.006$ in laboratory and field studies have also been observed to coincide with maximum N_2O fluxes and increasing production of N_2 fluxes (Friedl et al., 2018; Friedl et al., 2017; Owens et al., 2017; Rousset et al., 2020). A key determinant of a soil's D_p/D_o status are wetting-drainage cycles brought about by rainfall or irrigation events. Given that the frequency of irrigation and/or volume can potentially be manipulated to mitigate N_2O emissions (Mumford et al., 2019) and the fact that climate change may also lead to altered rainfall frequency and volumes it is important to better understand how soil D_p/D_o and associated N_2O emissions are affected by wetting-drainage cycles. To date the number of detailed studies that have examined the relationship between D_p/D_o and N_2O emissions remains limited, with few soil types examined, and no repeated wetting-drainage cycles. Thus, the objectives of this study were (i) to examine how successive

123 wetting and drainage cycles affected both modelled D_p/D_o dynamics and associated N_2O
124 emissions across soil bulk densities and (ii) to observe if these dynamics were influenced by
125 soil texture and density. We hypothesised that N_2O emissions would increase as D_p/D_o values
126 declined below 0.02 and peak at D_p/D_o values of 0.006, and that finer texture and greater soil
127 density would enhance N_2O emissions.

128

129 **2. Materials and methods**

130 *2.1 Soil collection and experimental design*

131 Two pasture soils were sampled (0-15 cm depth) in spring 2017: a Wakanui silt loam
132 soil, (Mottled Immature Pallic Soil), was collected from the dairy farm at Lincoln University
133 (43°38'41.3"S; 172°26'34.6"E); a well-drained Otorohanga loam soil, (Typic Orthic
134 Allophanic Soil), was collected at Ruakura, AgResearch, Hamilton (37°46'44.9"S
135 175°18'47.6"E). These soils were brought back to the laboratory and air-dried prior to sieving
136 (< 2 mm). Soil particle densities, particle sizes, particle size distribution and loss on ignition
137 were then determined. Soil particle density was determined (Flint and Flint, 2002) by placing
138 10 g of air-dry soil into a pycnometer that was then half filled with de-aired distilled water.
139 Any soil adhering to the inside of the neck of the pycnometer was washed down. The entrapped
140 air was removed by placing the pycnometer into a vacuum chamber and slowly applying a
141 vacuum, while being careful not to let the water bubble. De-aired water was then added to fill
142 the pycnometer and the stopper was inserted to expel excess water from the capillary.

143 The particle density (ρ_d) was calculated as follows:

144 $$\rho_d = \frac{[\rho_w(W_s - W_a)]}{[(W_s - W_a) - (W_{sw} - W_w)]} \quad [1]$$

where ρ_w is the density of water (g cm^{-3}) at the temperature observed, W_s is the weight of the pycnometer plus soil sample corrected to oven-dry water content (g), W_a is the weight of the pycnometer filled with air (g), W_{sw} is the weight of the pycnometer filled with soil and water (g), and W_w is the weight of the pycnometer filled with water (g) at the temperature of the observation. Particle size distribution was determined according to Kroetsch and Wang (2008) using a laser diffraction particle analyser (Mastersizer 3000, Malvern Panalytical). The uniformity coefficient (C_u), a measure of soil particle size variation, (Hazen 1892) and defined as the ratio of D_{60} to D_{10} was calculated (Figure S1). The value D_{60} is the particle size diameter at which 60% of soil particles are finer and 40% of soil particles are coarser, while D_{10} is the particle size diameter at which 10% of particles are finer and 90% of the particles are coarser. The coefficient D_{10} was determined by extrapolation using the inverse of the polynomial regressions for each soil (Figure S1). In addition, the percentage of soil aggregates passing through different sieve sizes (2.0, 1.4, 1.0 0.6 and 0.25 mm) for the Wakanui and Otorohanga soils was determined. Soil loss on ignition was determined at 500ºC (Blakemore et al., 1987). After determining the gravimetric water content of the air-dried soils, 24 soil cores were constructed by uniaxially compacting the air-dried soils inside stainless steel rings (7.3 cm internal diameter, 7.4 cm deep), to a depth of 4.1 cm. These soil cores were assigned to treatments according to the experimental design.

The experimental design consisted of two soils and three levels of bulk density for each soil type, replicated four times, giving 24 soil cores. Soil bulk density treatments for the Wakanui soil were 1.0, 1.1 and 1.2 Mg m^{-3}, while those for the Otorohanga soil were 0.9, 1.0, and 1.1 Mg m^{-3}. A lower soil bulk density was used for the Otorohanga soil because it could not be manually packed to a bulk density of 1.2 Mg m^{-3}. In addition, another 36 soil cores were made in order to perform destructive soil analyses on days 0 and 12 (2 soils x 3 bulk densities

169 x 3 replicates x 2 destructive sample times). The original 24 soil cores were destructively
170 sampled on day 25.

171 In order to evaluate both D_p/D_o dynamics and N_2O emissions, across successive
172 wetting-drainage cycles, six levels of soil matric potential (0, -2.0, -4.0, -6.0, -8.0 and -10.0
173 kPa) were used based on the earlier study of Rousset et al. (2020). To enable this tension tables
174 were prepared as described by Romano et al. (2002). Before placing soils cores on the tension
175 tables, deionised water was poured evenly across the tension tables to provide a good
176 connection between soil cores and the tension table. The tension tables were housed in a
177 laboratory where temperature fluctuations were negligible (20 ± 1ºC).

178 Prior to placing soil cores on the tension table, cores were saturated with a ^{15}N labelled
179 KNO_3 solution (300 µg N g^{-1} soil) with an enrichment of 50 atom% excess. This soil NO_3^-
180 concentration emulated the maximum typically found under bovine urine patches in grazed
181 pasture (e.g. Clough et al., 2009). The soil cores used for destructive sampling, on days 0 and
182 12, were treated similarly but with a KNO_3 solution at natural abundance. Once saturated the
183 soil cores were placed on the tension tables set at 0 kPa. Then, every 48 h soil drainage was
184 increased by adjusting the tension tables to the next drainage step, so that by day 12 the soil
185 cores had spent 48 h at -10 kPa. Upon the completion of one drainage cycle, soil drainage
186 ceased and the soil cores were returned to 0 kPa. To avoid cross contamination of NO_3^--^{15}N
187 enrichments, soil cores were placed into individual jars and wetted from the bottom up with
188 deionised water, prior to being placed back on the tension tables set at 0 kPa. The drainage
189 cycle was then repeated with drainage, once again, progressively increased every second day
190 so that by day 24 the soil cores had again been at -10 kPa for 48 h. Soil cores were weighed
191 daily, prior to any required adjustments to drainage settings.

192 Soil total porosity (ϕ; cm^3 pores cm^{-3} soil) was calculated as follows:

193 $$\phi = 1 - \left(\frac{\rho_b}{\rho_d}\right) \quad [2]$$

194 where ρ_d is the measured soil particle density (g cm^{-3}) and ρ_b is the soil bulk density (g cm^{-3}).

195 WFPS (%) and soil volumetric air content ε (cm^3 air cm^{-3} soil) were determined as follows:

196 $$WFPS = \frac{\theta_v}{\phi} \times 100 \quad [3]$$

197 $$\varepsilon = \phi - \theta_v \quad [4]$$

198 where θ_v is the soil volumetric water content (cm^3 water cm^{-3} soil).

199

200 *2.2 Determination of D_p/D_o, N_2O and N_2 fluxes*

201 Nitrous oxide fluxes were measured each day of the experiment using the ^{15}N enriched
202 soil cores. This was performed by removing the soil core from the tension table and placing it
203 in a 1 L mason jar which was then sealed with an air-tight lid equipped with a septum. Gas
204 samples (10 mL) were taken at 0, 20, and 40 min, after sealing the jar, using a 20 mL glass
205 syringe equipped with a 3-way stopcock and a 25G hypodermic needle. Gas samples were
206 injected into pre-evacuated 6 mL Exetainer® vials. Prior to analysis the gas samples were
207 brought to ambient pressure and analysed using a gas chromatograph (8610; SRI instruments,
208 Torrance, CA) connected to a Gilson autosampler (Gilson 222XL; Gilson, Middleton, WI) as
209 previously described (Clough et al., 2009). The change in the jar headspace N_2O concentration,
210 over time, was used to calculate the N_2O flux according to Hutchinson and Mosier (1981).
211 Cumulative N_2O emissions were calculated by manually integrating the daily fluxes over time.
212 On days 3, 4, 6, 8, 10, 12, 14, 16, 18, 22, and 24 gas samples (15 mL) were taken after 3 h, to
213 enable N_2 flux determinations, and placed in a 12 mL Exetainer® vial. The ^{15}N enrichments of
214 the N_2O and N_2 samples were determined on a continuous flow isotope ratio mass spectrometer
215 (Sercon 20/20; Sercon, Chesire, UK) according to the methodology of Mulvaney and Boast

(1986) and Stevens and Laughlin (2001). Replicated N_2O standards with ^{15}N enrichments of 0.366, 10.0 and 40.0 atom% were included in every batch of samples analysed. The N_2 flux detection limit (49 μg N m^{-2} h^{-1}) was determined using the between batch standard deviation (n = 100) of ambient air samples that equated to 9.1 x 10^{-6} and 4.1 x 10^{-5} for Δ29 and Δ30, respectively (Stevens and Laughlin 2001). Where Δ29 and Δ30 represent the differences between the molecular ratios of enriched and ambient atmospheres.

Using daily soil core mass, and prior knowledge of soil dry mass, particle density, and bulk density, values for ε were determined, as described above, and used to calculate D_p/D_o according to the SLWR model (Moldrup et al., 2013), as follows:

$$\frac{D_p}{D_o} = \varepsilon^{[1+C_m\emptyset]}\left(\frac{\varepsilon}{\emptyset}\right) \quad [5]$$

where C_m is the media complexity factor. As the experiment was performed using repacked soil, C_m was set to equal a value of 1 (Moldrup et al., 2013). The SWLR model was previously shown to have superior performance, relative to other models commonly used for predicting D_p/D_o in repacked soils (Moldrup et al., 2013). The SWLR model previously predicted well the measured D_p/D_o values from Rousset et al. (2020) for repacked Wakanui and Otorohanga soils with RMSE equal to 0.007 and 0.006, respectively, across a range of soil bulk densities (0.9 to 1.2) and matric potentials (0 to -10 kPa): similar or identical to those in the current study.

2.3 Destructive soil analyses

For destructive soil analyses, soil cores were first extruded into a Ziploc® plastic bag and mixed prior to a 10 g subsample being taken for gravimetric water content. This subsample was oven-dried at 105ºC for 24 h. Soil pH was measured using a calibrated flat surface pH electrode (Broadley James Corp., Irvine, CA.). Soil inorganic-N concentrations were

240 determined by extracting soil subsamples, the equivalent of 10 g of dry soil, with 100 mL of
241 2M KCl and shaking for 1 h. Then the extracts were filtered (Whatman 42), with the filtrate
242 analysed for NO_3^- and NH_4^+ on a flow injection analyser (Blakemore et al., 1987). To
243 determine dissolved organic carbon (DOC) a further soil subsample (equivalent of 5 g dry soil)
244 was extracted in 30 mL of deionised water by shaking for 30 minutes prior to centrifugation
245 (3,500 rpm for 20 minutes) and filtration (Whatman 42), with analyses performed on a
246 Shimadzu TOC analyser (Shimadzu, Oceania Ltd., Sydney, Australia).

247

248 *2.4 Statistical analyses*

249 Statistical analyses were performed using R studio (Version 1.1.447, RStudio Team
250 2016), also used to create the graphics presented using "ggplot2" package. Before any
251 statistical analysis were made, data were visually tested for normality, residual repartition and
252 the homoscedasticity. The function "shapiro.test" was used to double test the normality of the
253 residues. If the value of the Shapiro-Wilk Test was greater than 0.05, the data were considered
254 normal. If data deviated from a normal distribution then a log transformation was applied. A
255 repeated measures analysis, using ANOVA, was used to test differences between measured
256 variables, with Tukey's post-hoc test used to determine specific differences between means
257 with the least significant set to 5% level. Time (days of the experiment), soil types (2 levels:
258 Otorohanga and Wakanui) and soil ρ_b (3 levels per soil) were the explanatory variables.
259 Reported means are based on three or four replicates and error terms are the standard error of
260 the mean (s.e.m) as stated.

261

262 **3. Results**

263 *3.1 Soil physical and chemical characteristics*

The Wakanui soil had a greater percentage of clay and silt (Table 1) and a greater percentage of fine soil aggregates than the Otorohanga soil: on a gravimetric basis the Wakanui soil had 6.5 and 18.2% more aggregates passing through 0.6 and 0.25 mm sieves, respectively (Figure S1). The C_u value for the Wakanui soil was < 4 indicating a poorly graded/uniformly graded soil while the C_u for the Otorohanga soil was > 4 and diagnostic of a well graded soil having a well distributed range of particle sizes present (Hazen 1892). Soil pH remained stable throughout the experiment but was higher in the Wakanui soil (5.6 ± 0.1) compared to the Otorohanga soil (5.1 ± 0.1). The soil organic matter content was higher ($P < 0.05$) in the Otorohanga soil than in the Wakanui soil (Table 1). Conversely, soil DOC concentrations were higher ($P < 0.05$) in the Wakanui soil than in the Otorohanga soil when comparing individual sampling days (Figure 1; Table 2). In the Wakanui soil DOC did not vary with bulk density ($P = 0.373$) but did decline over time averaging 415, 249, and 161 μg C g^{-1} soil on days 0, 12, and 25, respectively, when averaged across bulk density treatment (Figure 1; Table 2). Similarly, soil bulk density did not affect DOC concentrations in the Otorohanga soil ($P = 0.140$), with no difference in DOC concentrations between days 0 and 12, however, lower DOC concentrations occurred at day 25 (Figure 1; Table 2).

Soil NO_3^--N concentrations were not affected by soil bulk density in the Wakanui soil, where they were highly variable at day 0, and declined from day 12 to day 25 (Figure 2; Table 2). A similar trend occurred in the Otorohanga soil (Figure 2; Table 2). The NH_4^+-N concentrations were 1 or 2 orders of magnitude less than the soil NO_3^- concentrations with few consistent differences over time. However, NH_4^+-N concentrations had decreased in the Wakanui soil by day 25 (Table 2).

Drainage increased ε, with higher values of ε in the Otorohanga soil at any given matric potential (Figure 3). There was no statistical effect of soil bulk density on ε in the Wakanui soil, but values of ε were higher in the Otorohanga soil at 0.9 Mg m^{-3} than at 1.0 or 1.1 Mg m^{-3}

289 ($P < 0.05$; Figure 3). Modelled values of D_p/D_o reflected these trends and differences in the ε
290 values with higher D_p/D_o in the Otorohanga soil (Figure 4). Modelled D_p/D_o increased
291 exponentially as a function of normalized air-filled porosity (ε/Φ), (Figure 4). The Otorohanga
292 soil generally had D_p/D_o values greater than recognised anaerobic thresholds while in the
293 Wakanui soil almost all D_p/D_o values were < 0.02, the threshold for the onset of anaerobic soil
294 conditions (Stepniewski, 1981), (Figure 4).

295

296 *3.2 N_2O and N_2 emission trends during drainage cycles*

297 Nitrous oxide fluxes peaked following commencement of drainage on days 2 and 3 in
298 the Otorohanga and Wakanui soils, respectively, (Figure 5, Figure 6) with respective fluxes of
299 28 and 145 mg m^{-2} h. However, fluxes were 5-fold higher in the Wakanui soil than the
300 Otorohanga soil. The N_2O fluxes then declined over time until day 12 whereupon the soil cores
301 were again saturated, causing the N_2O fluxes to increase again, regardless of soil type, before
302 declining with drainage. However, in the Wakanui soil the N_2O fluxes did not increase to the
303 same level as seen on day 2 with mean N_2O-N fluxes < 15 mg m^{-2} h on days 13-15 (Figure 5),
304 while in the Otorohanga soil the N_2O emissions after re-saturation of the soil closely followed
305 the lower N_2O flux trend observed over days 1 to 12 (Figure 6).

306 Nitrous oxide fluxes in the Wakanui soil, for the first drainage cycle, peaked at D_p/D_o
307 values of ~ 0.002 and as N_2O fluxes declined D_p/D_o increased until N_2O fluxes were near or
308 equal to zero at $D_p/D_o > 0.006$: this trend was repeated in the second drainage cycle (Figure 5).
309 Similar mirroring of the trends in the N_2O fluxes and D_p/D_o occurred in the Otorohanga soil,
310 but the peak N_2O fluxes coincided with D_p/D_o values close to 0.02 at soil bulk densities of 1.0
311 and 1.1, while at a soil bulk density of 0.9 the highest N_2O fluxes occurred over a D_p/D_o range
312 of 0.05 to 0.13 (Figure 6).

313 Comparing N_2O fluxes against WFPS showed that in the Wakanui soil N_2O fluxes
314 increased from 80% WFPS, with peak fluxes between 85-93% and 90-100% WFPS for the first
315 and second wetting-drainage cycles, respectively (Figure 7). In the Otorohanga soil N_2O fluxes
316 for soil bulk densities ≥1.0 Mg m^{-3} peaked at 76% and 64-68% WFPS for the first and second
317 wetting-drainage cycles, respectively: soil at 0.9 Mg m^{-3} had peak N_2O at WFPS values of 58%
318 and 44% for the first and second wetting-drainage cycles, respectively (Figure 8).

319 Cumulative N_2O-N fluxes, from day 1 to 24, were higher ($P < 0.01$) in the Wakanui
320 than the Otorohanga soil (Figure S2). There was no effect of soil bulk density on cumulative
321 N_2O-N fluxes in the Wakanui soil but in the Otorohanga soil lower cumulative fluxes ($P <$
322 0.05) occurred in the 0.9 Mg m^{-3} bulk density treatment when compared to the 1.0 and 1.1 Mg
323 m^{-3} treatments (Figure S2).

324 The ^{15}N enrichment of the N_2O-N was highest in the Wakanui soil during the first
325 drainage cycle decreasing from a mean value of 26.0 atom% on day 3, averaged across soil
326 bulk densities, to a mean of 13.6 atom% prior to re-saturation of the soil on day 12. After re-
327 saturation the ^{15}N enrichment of the N_2O flux increased on day 14 to a mean value of 16.0
328 atom% before declining again to be 3.7 atom% on day 24 (Figure 9). There were few
329 differences in N_2O-^{15}N enrichment due to soil bulk density in the Wakanui soil. In the first
330 drainage cycle the Otorohanga soil N_2O-^{15}N enrichment was initially 4.0 atom% on day 1
331 before increasing to 7.4 atom% on day 6 where after values declined over time to average 5.6
332 atom% on day 24 at bulk densities of 1.0 or 1.1 Mg m^{-3}, and 4.1 atom% at a bulk density of 0.9
333 Mg m^{-3} (Figure 9). The N_2O-^{15}N enrichments in the 0.9 Mg m^{-3} treatment were generally lower
334 ($P < 0.01$) than in the other bulk densities for the Otorohanga soil (Figure 9).

335 Soil N_2 fluxes in the Wakanui soil peaked on day 6 (1.8 mg N m^{-2} h^{-1}) and 16 (4.5 mg
336 N m^{-2} h^{-1}) during the first and second drainage cycles (Figure 10), respectively: these N_2 peak
337 fluxes were one or two orders of magnitude lower than the peak N_2O-N fluxes with few

differences due to bulk density. Fluxes of N_2 from the Otorohanga soil were an order of magnitude lower than those observed in the Wakanui soil (Figure 10). Fluxes of N_2 varied sporadically with soil bulk density treatment in the Otorohanga soil until day 14 when N_2 flux increased regardless of soil bulk density (Figure 10). At 0.9 Mg m^{-3} the soil N_2 flux then declined relatively slowly, while at soil bulk densities of 1.0 and 1.1 Mg m^{-3} N_2 fluxes declined by day 16 before they again increased (Figure 10).

4. Discussion

Although the Otorohanga soil had a lower particle density, the total porosity was only 2-3% higher than the Wakanui soil at comparable bulk densities (1.0 and 1.1 Mg m^{-3}). However, the fact that the Otorohanga soil's air-filled porosity values were consistently higher, at any given matric potential, demonstrates that the Otorohanga soil contained a higher percentage of macropores (pores with a diameter > 30 μm) since macropores drain at matric potentials over the range of 0 to -10 kPa (Schjønning et al., 2003). Greater macroporosity in the Otorohanga soil resulted from there being a well distributed range of particle sizes present (C_u > 4) with coarser texture and fewer soil aggregates < 0.6 mm in size. At the lower bulk density of 0.9 Mg m^{-3} in the Otorohanga soil the macroporosity was higher still due to reduced aggregate damage, as a consequence of reduced compaction, resulting in the observed enhanced air-filled porosity. The higher occurrence of air-filled macropores in the Otorohanga soil consequently caused a greater proportion of the total porosity to be air-filled and explains the higher values of D_p/D_o determined in the Otorohanga soil.

The higher air-filled porosity in the Otorohanga soil equated with higher normalised air-filled porosities which explains why the majority of the Otorohanga soil D_p/D_o values were above Stepniewski's (1981) anaerobic limit of 0.02, where plants roots are considered to begin experiencing anaerobiosis, and the previously described threshold for peak N_2O emissions of 0.006 (Balaine et al., 2013). Conversely, the finer texture and higher percentage of finer

aggregates in the Wakanui soil reduced macroporosity, increasing microporosity, causing most D_p/D_o values to be < 0.02, and with the majority < 0.006. Consequently, the soil matric potentials applied across the wetting-drainage cycles resulted in varying D_p/D_o regimes that affected N_2O fluxes accordingly.

During the first wetting-drainage cycle, maximum N_2O fluxes following saturation in the Wakanui soil, coincided with D_p/D_o values < 0.006, with the observed decline in the N_2O fluxes corresponding with increased drainage and the ensuing increase in soil O_2, as manifested in the higher D_p/D_o values (> 0.006). Contrary to the hypothesis, the D_p/D_o values associated with peak N_2O emission were either below (Wakanui soil) or above (Otorohanga soil) the D_p/D_o value of 0.006 that was previously shown to correspond with peak N_2O emissions (Balaine at al., 2013; 2016). In the Wakanui soil peak N_2O emissions at D_p/D_o values < 0.006 may have resulted from relatively high soil NO_3^- concentrations favouring N_2O production over N_2 formation, as discussed below. While in the Otorohanga soil the fact N_2O emissions, which were relatively low compared to the Wakanui soil, peaked at D_p/D_o values indicative of aerobic soil conditions indicates other processes (e.g. nitrification or nitrifier-denitrification) generated the N_2O evolved or that the higher organic matter content of the Otorohanga soil was generating a greater O_2 demand and inducing anaerobic conditions at relatively higher values of *Dp/Do* (Petersen et al., 2013; Rohe et al., 2021). The elevated ^{15}N enrichment of the N_2O demonstrates that the ^{15}N labelled NO_3^- contributed strongly to the N_2O flux in the Wakanui soil but this enrichment declined as the drainage cycle progressed, demonstrating that the N_2O-N source was being diluted as a consequence of mineralization and nitrification of antecedent-N. In the Otorohanga soil the 5-fold lower fluxes can be attributed to conditions less suitable for anaerobic production of N_2O due to the higher D_p/D_o values.

In the current experiment, given the relatively low SOC content of the Wakanui soil, the observed DOC concentrations, and the relatively high soil NO_3^- concentrations, it can be

388 assumed that denitrification was predominately responsible for the N_2O fluxes when soil D_p/D_o
389 was < 0.006. This is further evidenced by the generation of N_2 on day 6, following the decline
390 in the N_2O flux. Time lags in N_2 fluxes relative to the peak N_2O fluxes, in the Wakanui soil,
391 result from the need for N_2O reductase to be formed, a process that varies between soils. Some
392 pasture soils perform concurrent N_2O production and reduction from commencement of
393 anaerobic conditions, while others perform the steps sequentially with N_2O production
394 complete prior to stoichiometric conversion to N_2 (Highton et al., 2020). Also contributing to
395 the lag over the course of a drainage cycle is the fact that N_2 cannot diffuse from the soil until
396 the air-entry potential of the soil, which facilitates gas diffusion, has been achieved (Balaine et
397 al., 2013): O_2 entry into the soil causes denitrification to decline while any entrapped
398 denitrification products are able to diffuse out of the soil. Thus, if N_2O had been converted to
399 N_2 at depth in the soil core it will not have generated a soil surface flux until the air entry point
400 was reached, further into the drainage cycle, than N_2O fluxes being generated at a shallower
401 soil depth and where diffusion of N_2O from the soil may have been sooner in time.

402 Previously, N_2O concentrations have been observed to peak at D_p/D_o values of 0.006
403 with N_2O reduction and enhanced N_2 fluxes increasing at values < 0.006, unless the N_2 is
404 entrapped (Balaine et al., 2013, 2016). While there was lag in peak N_2 fluxes in the Wakanui
405 soil, for reasons noted above, the size of the N_2 flux was lower relative to the N_2O flux. This
406 may have been the result of the abundant NO_3^- supply. Under anaerobic conditions, the
407 addition of NO_3^- can alter the $N_2O/(N_2O+N_2)$ ratio (Liu et al., 2013; Scheer et al., 2016;
408 Senbayram et al., 2012). A two-year field study by Qin et al. (2017) showed that elevated NO_3^-
409 concentrations averaging 30 mg kg^{-1} (range 17-58 mg kg^{-1}) were sufficient to consistently
410 increase the $N_2O/(N_2+N_2O)$ ratio. Based on this the soil NO_3^- concentrations in the current
411 experiment were sufficient to impede N_2O reductase. Furthermore, the relatively low soil pH
412 values may have hindered the function of N_2O reductase. For example, Čuhel et al. (2010)

found acidic soils (pH average 5.52) increased the $N_2O/(N_2O + N_2)$ ratio and were unfavourable for N_2O reduction to N_2. This occurs because acidic soils diminish or prevent reduction of N_2O by impeding the assembly of functional N_2O reductase (Liu et al., 2014). The reduction of N_2O to N_2 has been shown to be relatively slow in soils with a pH < 6.4, increasing between pH between 6.4 and 6.8, and becoming fully functional at pH > 6.8 (Hénault et al., 2019).

While the highest N_2O fluxes again aligned with D_p/D_o values < 0.006 during the Wakanui soil's second wetting-drainage cycle these fluxes were an order of magnitude lower than in the first wetting-drainage cycle. The D_p/D_o values indicate anaerobic pathways were again responsible for the N_2O fluxes. The fact that the N_2O fluxes were an order of magnitude lower in the second drainage cycle possibly indicates a lower rate of N_2O production, which is unlikely given the anaerobic conditions and NO_3^- substrate supply. However, the DOC content at day 12 had declined, and the relative quality of the DOC available was unknown, thus, these factors could have reduced N_2O production.

Temporal declines in the ^{15}N enrichment of the soil NO_3^- pool, indicative of concurrent soil derived NO_3^- formation, have been reported for both temperate and subtropical pasture or grassland soils (Rutting et al., 2010; Muller et al., 2014; Moser et al., 2018; Friedl et al., 2018). Both heterotrophic and autotrophic nitrification processes may be responsible for NO_3^- production and the dominance of either process depends on a soil's aeration status and texture. For example, upon incubating soils (25ºC over 2 days) of varying texture, Friedl et al. (2018) found heterotrophic nitrification dominated the production of NO_3^- when WFPS was 95% in both a clay and a sandy soil, while in a loam it dominated at all WFPS values (40-95%), autotropic nitrification peaked at 60% WFPS in clay and sandy soils. The dilution of a given NO_3^- pool by ongoing nitrification processes can be rapid following soil rewetting, with gross nitrification rates of > 20 μg g^{-1} soil day^{-1} reported for subtropical pasture soil (Friedl et al., 2018). At cooler temperatures the dilution rate may decrease, for example, Thomas et al. (2019)

438 applied weekly wetting-drainage cycles to intact silt loam soil cores receiving 250 kg N ha^{-1} as
439 KNO_3, maintained at 14°C over 74 days, and observed a gradual decline in the ^{15}N atom% of
440 N_2O from ~48 to ~20 atom%. Hence, the temporal decline in the N_2O-^{15}N enrichment in the
441 Wakanui soil, indicative of the ^{15}N enrichment of the denitrifying pool can be attributed to
442 nitrification of antecedent soil N, as noted previously by Thomas et al. (2019) using a temperate
443 soil of similar texture and organic matter content. This highlights the difficulty of attempting
444 to measure N_2 fluxes over time when the ^{15}N enrichment of the denitrifying pool also declines
445 with time. The method of Mulvaney and Boast (1986) used for calculating N_2 fluxes assumes
446 that the ^{15}N labelled NO_3^- pool undergoing denitrification exists as a single pool that is
447 isotopically uniform. Failure to meet this assumption may result in underestimation of the N_2
448 flux. Clearly, as evidenced by the initially low (Otorohonga soil) and declining enrichment of
449 the N_2O derived (Wakanui soil), there were multiple pools of NO_3^- either initially present or
450 being formed as a result of mineralisation and nitrification. Thus, N_2 fluxes may have been
451 underestimated as result of this assumption not being met. The recovery of NO_3^- in the KCl
452 extractions, especially at time zero in the Otorohonga soil, indicates uneven distribution of
453 NO_3^- in the soil core profiles: the soil subsample represented ~ 6% by weight of the total soil
454 mass in the repacked soil core and low soil NO_3^- concentrations at this time suggest poor
455 homogenisation of the soil sample or possible macropore flow of solution generating uneven
456 distribution.

457 The N_2O fluxes in the Otorohanga soil increased during drainage at soil D_p/D_o values
458 generally considered aerobic (> 0.02): at bulk densities of 1.0 and 1.1 Mg m^{-3} the N_2O fluxes
459 began to increase at a D_p/D_o value ~0.05 while at a bulk density of 0.9 Mg m^{-3} peak N_2O fluxes
460 generally occurred between D_p/D_o 0.05 and 0.10. The applied NO_3^--^{15}N made a much lower
461 contribution to the N_2O flux than in the Wakanui soil; indicating that antecedent soil N
462 comprised a significant portion of the N_2O evolved.

While soil drainage conditions and resulting D_p/D_o values indicated that the Otorohanga soil's inter-aggregate pore space was aerobic the drainage applied was not sufficient to drain the intra-aggegrate pore space (Jayarathne et al., 2020) where anaerobic conditions may have existed during wetting-drainage cycles. Silt loam aggregates (43% gravimetric water content) with radii ≤ 6 mm were shown to have aerobic centres when incubated in air (Sexstone et al., 1985). In the current experiment aggregates were ≤ 2 mm, however, it is still conceivable that these aggregates had anaerobic centres as a consequence of soil wetting reducing the O_2 supply or the demand for O_2 being sufficiently high to induce anaerobic conditions in the intra-aggregate pore space. Given that N_2O fluxes in the Otorohanga soil, where aggregates were all ≤ 2 mm, were highest over the first 5 days of drainage it is possible that aggregates only became fully aerobic after macropore drainage allowed O_2 to diffuse into water-filled intra-aggregate pores. Hence anaerobic or hypoxic conditions within the intra-aggregate zone may have facilitated the contribution of NO_3^--^{15}N to N_2O production. Alternatively, the O_2 demand may have increased due to wetting and draining generating microbial substrates. For example, Petersen et al. (2013) recorded N_2O emissions from cropping system soils at D_p/D_o > 0.02 following a simulated freeze-thaw cycle, and attributed this to an increased O_2 demand, due to inputs of C from crop residues, generating anaerobic conditions. While, similar to the Otorohanga soil, Friedl et al. (2018) also observed N_2 fluxes at D_p/D_o values > 0.02 due to the wetting up of dry pasture soil releasing C and N. In their ^{15}N tracing study Friedl et al. (2018) were able to show that the wetting of dry pasture soil increased DNRA, with both DNRA and denitrification responding positively to NO_3^- supply, with increasing heterotrophic respiration generating a reduction in the redox potential which in turn shifted NO_3^- consumption from denitrification to DNRA. Increasing soil organic matter content can improve soil aggregation, and thus diffusivity, and this explains the well graded aggregate structure of the Otorohonga soil. This organic matter can also provide C for heterotrophic denitrifiers and increase soil

488 water retention. Notably, the soil organic C concentration was lower, but the DOC level was
489 higher, in the Wakanui soil compared to the Otorohanga soil, indicating different organic
490 matter quality. Thus, differences in organic matter quality may also have contributed to
491 differences in N_2O emissions between soils by altering soil O_2 demand. Using repacked soil
492 cores Rohe et al. (2021) found that gaseous N emissions were well predicted when considering
493 both O_2 supply and demand, with the latter based on CO_2 emissions and the anaerobic soil
494 volume fraction. However, basing O_2 demand solely on SOM content as a proxy for O_2 demand
495 reduced the ability to predict gaseous N emissions from repacked soil (Rohe et al. 2021). The
496 current study does not permit delineation of microbial pathways for N_2O generation but it is
497 possible that redox effects similar to those observed by Friedl et al. (2018) also occurred,
498 especially given the higher soil organic matter content. Dilution of the applied NO_3^--^{15}N
499 enrichment, assumed to match that of the N_2O-^{15}N enrichment, was initially greater in the
500 Otorohanga soil than in the Wakanui soil potentially due to a higher level of soil organic matter
501 elevating the contribution of the antecedent NO_3^--N pool more in the Otorohanga soil. Friedl
502 et al. (2018) observed higher rates of NO_3^- production, dominated by heterotrophic nitrification
503 in clay and loam soils while lower net nitrification rates occurred in a sandy clay loam
504 dominated by autotrophic nitrification. Thus, the Otorohanga soil loam may have had greater
505 heterotrophic nitrification occurring. Under hypoxic conditions nitrifiers may also perform
506 nitrifier-denitrification to generate N_2O (Stein, 2019) and NO_3^--^{15}N, transformed to NO_2^-, may
507 have also contributed to N_2O-^{15}N via this process.

508 In conclusion, soil texture and structure affected soil drainage rate and residual soil
509 moisture, both of which influenced active pore space for gas diffusion (D_p/D_o). The results
510 confirm that values of D_p/D_o indicative of anaerobic conditions result in higher N_2O emissions,
511 but that the magnitude of the N_2O flux may not be consistent over repeated wetting-drainage
512 cycles. Reasons for the reduction of the N_2O flux in repeat wetting-drainage cycles require

513 further investigation and should examine the potential for a shift in microbial N_2O production
514 mechanisms as a result of soil redox dynamics. Soil O_2 demand may also reduce soil redox in
515 soils with high organic matter contents following wetting-drainage events and future work
516 should aim to characterise the relationship between soil organic matter, changes in redox and
517 N_2O production mechanisms over successive wetting-draining events. Conversely,
518 reproducible, but 5-fold lower N_2O fluxes were observed from a loam soil, during successive
519 wetting-draining events, with soil structure generating D_p/D_o values indicative of aerobic
520 conditions within macropores, and where antecedent soil N source dominated the N_2O-N
521 source. Results implicate the intra-aggregate pore space as a zone for anaerobic or hypoxic
522 N_2O generation pathways during drainage and should be further investigated.

523

524 **5 Acknowledgements**

525 The authors gratefully acknowledge funding (SOW14-GPLER-SP198-LIN) from the
526 New Zealand Fund for Global Partnerships in Livestock Emissions Research (GPLER), an
527 international research fund set up by the New Zealand Government in support of the Global
528 Research Alliance on Agricultural Greenhouse Gases (GRA).

529

530 **References**

531 Balaine, N., Clough, T.J., Beare, M.H., Thomas, S.M., Meenken, E.D., 2016. Soil Gas
532 Diffusivity Controls N_2O and N_2 Emissions and their Ratio. Soil Sci. Soc. Am. J. 80(3), 529-
533 540. https://doi:10.2136/sssaj2015.09.0350.

534 Balaine, N., Clough, T.J., Beare, M.H., Thomas, S.M., Meenken, E.D., Ross, J.G., 2013.
535 Changes in Relative Gas Diffusivity Explain Soil Nitrous Oxide Flux Dynamics. Soil Sci. Soc.
536 Am. J. 77, 1496-1505. https://doi:10.2136/sssaj2013.04.0141.

537 Blakemore, L.C., Searle, P.L., Daly, B.K., 1987. Methods for chemical analysis of soils. New
538 Zealand Soil Bureau report, 80. Manaaki-Whenua Press, Lincoln, New Zealand.

539 Ciais, P., Sabine, C., Bala, G., Bopp, L., Brovkin, V., Canadell, J., Chhabra, A., DeFries, R.,
540 Galloway, J., Heimann, M., Jones, C., Le Quéré, C., Myneni, R.B., Piao, S., Thornton, P.E.,
541 2013. Carbon and Other Biogeochemical Cycles. In: Climate Change 2013: The Physical
542 Science Basis. Contribution of Working Group I to the Fifth Assessment Report of the
543 Intergovernmental Panel on Climate Change. Cambridge University Press, Cambridge, United
544 Kingdom.

545 Clough, T.J., Ray, J.L., Buckthought, L.E., Calder, J., Baird, D., O'Callaghan, M., Sherlock,
546 R.R., Condron, L.M., 2009. The mitigation potential of hippuric acid on N_2O emissions from
547 urine patches: An in situ determination of its effect. Soil Biol. Biochem. 41, 2222-2229.
548 https://doi:10.1016/j.soilbio.2009.07.032.

549 Čuhel J., Šimek M., Laughlin R.J., Bru D., Chèneby D., Watson C.J., Philippot L., 2010.
550 Insights into the Effect of Soil pH on N_2O and N_2 Emissions and denitrifiers community size
551 and activity. Ap. and Env. Micro. 76, 1870–1878. https://doi:10.1128/AEM.02484-09.

552 Davidson, E.A., 2009. The contribution of manure and fertilizer nitrogen to atmospheric nitrous
553 oxide since 1860. Nature Geosciences 2, 659-662. https://doi:10.1038/ngeo608.

554 Erisman, J.W., Galloway, J., Seitzinger, S., Bleeker, A., Butterbach-Bahl, K., 2011. Reactive
555 nitrogen in the environment and its effect on climate change. Current Opinion in Environmental
556 Sustainability 3, 281-290.

557 Farquharson R., Baldock J., 2007. Concepts in modelling N_2O emissions from land use. Plant
558 and Soil 309, 147–167. https://doi:10.1007/s11104-007-9485-0.

559 Friedl, J., De Rosa, D., Rowlings, D.W., Grace, P.R., Müller, M., Scheer, C., 2018.
560 Dissimilatory nitrate reduction to ammonium (DNRA), not denitrification dominates nitrate

561 reduction in subtropical pasture soils upon rewetting. Soil Biol. Biochem. 125, 340-349.
562 https://doi:10.1016/j.soilbio.2018.07.024.

563 Friedl, J., Scheer, C., Rowlings, D.W., Mumford, M.T., Grace, J., 2017. The nitrification
564 inhibitor DMPP (3,4-dimethylpyrazole phosphate) reduces N_2 emissions from intensively
565 managed pastures in subtropical Australia. Soil Biol. Biochem. 108, 55-64.
566 https://doi:10.1016/j.soilbio.2017.01.016.

567 Hao, X., Ball, B.C., Culley, J.L.B., Carter, M.R., Parkin, G.W., 2008. Soil Density and
568 Porosity. In: M.R. Carter, E.G. Gregorich (Eds.), Soil sampling and methods of analysis. Taylor
569 & Frabcis, Boca Raton, FL., pp. 743-759.

570 Hazen A., 1892. Some physical properties of sands and gravels: With special reference to their
571 use in filtration.

572 Hénault, C., Bourennane, H., Ayzac, A., Ratié, C., Saby, N.P.A., Cohan, J.P., Eglin, T., Gall,
573 C.L., 2019. Management of soil pH promotes nitrous oxide reduction and thus mitigates soil
574 emissions of this greenhouse gas. Scientific Reports 9, 1–11. https://doi.org/10.1038/s41598-
575 019-56694-3

576 Highton M.P., Bakken L.R., Dörsch P., Wakelin S., de Klein C.A.M., Molstad L., Morales
577 S.E., 2020. Soil N_2O emission potential falls along a denitrification phenotype gradient linked
578 to differences in microbiome, rainfall and carbon availability. Soil Biol. Biochem. 150, 108004.
579 https://doi:10.1016/j.soilbio.2020.108004.

580 Hutchinson, G.L., Mosier, A.R., 1981. Improved soil cover method for field measurement of
581 nitrous oxide fluxes. Soil Sci. Soc. Am. J. 45, 311-316.
582 https://doi:10.2136/sssaj1981.03615995004500020017x.

583 Kroetsch, D., Wang, C., 2008. Particle Size Distribution. In: M.R. Carter, E.G. Gregorich
584 (Eds.), Soil Sampling and Methods of Analysis. CRC Press. Taylor & Francis Group., Boca
585 Raton, FL.

586 Jayarathne J.R.R.N., Chamindu Deepagoda T.K.K., Clough T.J., Nasvi M.C.M., Thomas S.,
587 Elberling B., Smits K., 2020. Gas-Diffusivity based characterization of aggregated agricultural
588 soils. Soil Sci. Soc. Am. J. 84, 387–398. https://doi:10.1002/saj2.20033.

589 Linn D.M., Doran J.W., 1984. Effect of Water-Filled Pore Space on Carbon Dioxide and
590 Nitrous Oxide Production in Tilled and Nontilled Soils. Soil Sci. Soc. Am. J. Journal 48, 1267–
591 1272. https://doi:10.2136/sssaj1984.03615995004800060013x.

592 Liu B., Frostegård Å., Bakken L.R., 2014. Impaired reduction of N_2O to N_2 in acid soils is due
593 to a posttranscriptional interference with the expression of nosZ. mBio 5,.
594 doi:10.1128/mBio.01383-14.

595 Liu, B., Mao, Y., Bergaust, L., Bakken, L.R., Frostegård, A., 2013. Strains in the genus Thauera
596 exhibit remarkably different denitrification regulatory phenotypes. Environ. Microbiol. 15(10),
597 2816-2828. https://doi:10.1111/1462-2920.12142

598 Moldrup, P., Chamindu Deepagoda, T.K.K., Hamamoto, S., Komatsu, T., Kawamoto, K.,
599 Rolston, D.E., Wollesen de Jonge, L., 2013. Structure-Dependent Water-Induced Linear
600 Reduction Model for Predicting Gas Diffusivity and Tortuosity in Repacked and Intact Soil.
601 Vadose Zone J. 12, 2-11. https://doi:10.2136/vzj2013.01.0026.

602 Moser, G., Gorenflo, A., Brenzinger, K., Keidel, L., Braker, G., Marhan, S., Clough, T.J.,
603 Muller, C., 2018. Explaining the doubling of N_2O emissions under elevated CO_2 in the Giessen
604 FACE via in-field N-15 tracing. Glob. Change Biol 24, 3897-3910.
605 https://doi:10.1111/gcb.14136.

606 Muller, C., Laughlin, R.J., Spott, O., Rutting, T., 2014. Quantification of N_2O emission
607 pathways via a N-15 tracing model. Soil Biol. Biochem. 72, 44-54.
608 https://doi:10.1016/j.soilbio.2014.01.013.

609 Mulvaney, R.L., Boast, C.W., 1986. Equations for determination of nitrogen-15 labelled
610 dinitrogen and nitrous oxide by mass spectrometry. Soil Sci. Soc. Am. J. 50, 360-363.
611 https://doi:10.2136/sssaj1986.03615995005000020021x.

612 Mumford, M.T., Rowlings, D.W., Scheer, C., De Rosa, D., Grace, P.R., 2019. Effect of
613 irrigation scheduling on nitrous oxide emissions in intensively managed pastures. Agr. Ecosyst.
614 Environ. 272, 126-134. https://doi:10.1016/j.agee.2018.11.011.

615 Owens, J., Clough, T.J., Laubach, J., Hunt, J.E., Venterea, R.T., 2017. Nitrous Oxide Fluxes
616 and Soil Oxygen Dynamics of Soil Treated with Cow Urine. Soil Sci. Soc. Am. J. 81, 289-298.
617 https://doi:10.2134/jeq2015.10.0516.

618 Pandey, A., Suter, H., He, J., Hu, H., Chen, D., 2019. Dissimilatory nitrate reduction to
619 ammonium dominates nitrate reduction in long-term low nitrogen-fertilized rice studies. Soil
620 Biol. Biochem. 131, 149-156. https://doi:10.1016/j.soilbio.2019.01.007.

621 Petersen, S.O., Ambus, P., Elsgaard, L., Schjønning, P., Olesen, J.E., 2013. Long-term effects
622 of cropping system on N_2O emission potential. Soil Biol. Biochem. 57, 706-712.
623 https://doi:10.1016/j.soilbio.2012.08.032.

624 Petersen, S.O., Schjønning, P., Thomsen, I.K., Christensen, B.T., 2008. Nitrous oxide
625 evolution from structurally intact soil as influenced by tillage and soil water content. Soil Biol.
626 Biochem. 40, 967-977. https://doi:10.1016/j.soilbio.2007.11.017.

627 Qin, S.P., Ding, K.R., Clough, T.J., Hu, C.S., Luo, J.F., 2017. Temporal in situ dynamics of
628 N_2O reductase activity as affected by nitrogen fertilization and implications for the $N_2O/(N_2O+$

629 N_2) product ratio and N_2O mitigation. Biol. Fert. Soils 53, 723-727.
630 https://doi:10.1007/s00374-017-1232-y.

631 Ravishankara, A.R., Daniel, J.S., Portmann, R.W., 2009. Nitrous Oxide (N_2O): The Dominant
632 Ozone-Depleting Substance Emitted in the 21st Century. Science 326, 123-125.
633 https://doi:10.1126/science.1176985.

634 Reddy, K.R., DeLaune, R.D., 2008. Biogeochemistry of Wetlands: Science and Applications
635 (1st ed.). CRC Press. https://doi.org/10.1201/9780203491454

636 Rohe, L., Apelt, B., Vogel, H.J., Well, R., Wu, G.M., Schlüter, S., 2021. Denitrification in soil
637 as a function of oxygen availability at the microscale. Biogeosciences, 18, 1185–1201.
638 https://doi.org/10.5194/bg-18-1185-2021

639 Rolston, D.E., Moldrup, P., 2012. Gas Transport in Soils. In: P.M. Huang, Y. Li, M.E. Sumner
640 (Eds.), Handbook of Soil Sciences Properties and Processes Second Edition. Taylor & Francis
641 Group, Boca Raton, FL., pp. 8-1.

642 Romano, N., Hopmans, J.W., Dane, G.H., 2002. Water retention and storage. In: G.C. Topp,
643 G.H. Dane (Eds.), Methods of Soil Analysis, Part 4, Physical Methods. Soil Sci. Soc. Am. J.,
644 Madison, WI, pp. 692-698.

645 Rousset C., Clough T.J., Grace P.R., Rowlings D.W., Scheer C., 2020. Soil type, bulk density
646 and drainage effects on relative gas diffusivity and N_2O emissions. Soil Res.
647 https://doi:10.1071/SR20161.

648 RStudio Team. 2016. RStudio: Integrated Development for R. http://www.rstudio.com/

649 Rutting, T., Clough, T.J., Muller, C., Lieffering, M., Newton, P.C.D., 2010. Ten years of
650 elevated atmospheric carbon dioxide alters soil nitrogen transformations in a sheep-grazed
651 pasture. Glob. Change Biol. 16, 2530-2542. https://doi:10.1111/j.1365-2486.2009.02089.x.

652 Scheer, C., Meier, R., Brüggemann, N., Grace, P.R., Dannenmann, M., 2016. An improved ^{15}N
653 tracer approach to study denitrification and nitrogen turnover in soil incubations. Rapid
654 Commun. Mass Spectrom. 30, 2017-2026. https://doi.org/10.1002/rcm.7689

655 Schjønning, P., Thomsen, I.K., Moldrup, P., Christensen, B.T., 2003. Linking Soil Microbial
656 Activity to Water- and Air-Phase Contents and Diffusivities. Soil Sci. Soc. Am. J. 67, 156-165.
657 https://doi:10.2136/sssaj2003.1560.

658 Senbayram, M., Chen, R., Budai d, A., Bakken, L., Dittert, K., 2012. N_2O emission and the
659 $N_2O/(N_2O + N_2)$ product ratio of denitrification as controlled by available carbon substrates
660 and nitrate concentrations. Agr. Ecosys. & Environ 147, 4-12.
661 https://doi:10.1016/j.agee.2011.06.022.

662 Sexstone A.J., Revsbech N.P., Parkin T.B., Tiedje J.M., 1985. Direct Measurement of Oxygen
663 Profiles and Denitrification Rates in Soil Aggregates. Soil Sci. Soc. Am. J. 49, 645–651.
664 https://doi:10.2136/sssaj1985.03615995004900030024x.

665 Stein L.Y., 2019. Insights into the physiology of ammonia-oxidizing microorganisms. Curr.
666 Opin. Chem. Boil. 49, 9–15. https://doi:10.1016/j.cbpa.2018.09.003.

667 Stepniewski, W., 1981. Oxygen diffusion and the strength as related to soil compaction. II
668 Oxygen diffusion coefficient. Pol. J. Soil Sci. 14, 3-13.

669 Stevens, R.J., Laughlin, R.J., 2001. Lowering the detection limit for dinitrogen using the
670 enrichment of nitrous oxide. Soil Biol. Biochem. 33, 1287-1289. https://doi:10.1016/S0038-
671 0717(01)00036-0.

672 Thomas, S.M., Fraser, P.M., Hu, W., Clough, T.J., Van Der Klei, G., Wilson, S., Tregurtha,
673 R., Baird, D., 2019. Tillage, compaction and wetting effects on NO_3, N_2O and N_2 losses.
674 https://doi:10.1071/SR18261.

675 Van den Berg, E.M., Boleij, M., Kuenen, J.G., Kleerebezem, R., van Loosdrecht, M., 2016.
676 DNRA and denitrification coexist over a broad range of acetate/N-NO_3^- ratios, in a chemostat
677 enrichment culture. Front. Microbiol. 7, 1842. https://doi:10.3389/fmicb.2016.01842.

678 Wrage-Mönnig, N., Horn, M.A., Well, R., Muller, C., Velthof, G., Oenema, O., 2018. The role
679 of nitrifier denitrification in the production of nitrous oxide revisited. Soil Biol. Biochem. 123,
680 A3-A16. https://doi:10.1016/j.soilbio.2018.03.020.

681 Wrage, N., Velthof, G.L., van Beusichem, M.L., Oenema, O., 2001. Role of nitrifier
682 denitrification in the production of nitrous oxide. Soil Biol. Biochem. 33, 1723-1732.
683 https://doi:10.1016/S0038-0717(01)00096-7.

684

685 LIST OF CAPTIONS

686

687 Figure 1. Mean dissolved organic carbon content (DOC) for the Wakanui and Otorohanga
688 soils at the beginning of the experiment (Day 0), after the end of the first wetting-drainage
689 cycle (Day 12) and at the end of the second wetting-drainage cycle (Day 25). Numerals in the
690 legend indicate the soil bulk density treatments applied (Mg m^{-3}). Error bar = s.e.m; n=4 on
691 day 25, n=3 on days 0 and 12.

692 Figure 2. Mean nitrate (NO_3^--N) concentrations for the Wakanui and Otorohanga soils at
693 the beginning of the experiment (Day 0), after the end of the first wetting-drainage cycle (Day
694 12) and at the end of the second wetting-drainage cycle (Day 25). Numerals in the legend
695 indicate the soil bulk density treatments applied (Mg m^{-3}). Error bar = s.e.m; n=4 on day 25,
696 n=3 on days 0 and 12.

697

698 Figure 3. Soil air content (Ɛ), as a function of relative matric potentials (-kPa) for the
699 Wakanui and Otorohanga soils, averaged over the two wetting-drainage cycles. Numerals in
700 the legend indicate the soil bulk density treatments applied (Mg m^{-3}). Error bar = s.e.m; n=8.
701 Note the different scales for the y-axis.

702

703 Figure 4. Soil-gas diffusivity (D_p/D_o), as a function of relative air-filled porosity (Ɛ/Φ)
704 for the Wakanui and the Otorohanga soils. Also shown are the previously reported gas
705 diffusivity values for peak N_2O fluxes at $D_p/D_o = 0.006$ (– – – –; Balaine et al., 2013) and onset
706 of anaerobic conditions D_p/D_o = 0.02 (------; Stepniewski 1981). Numerals in the legend
707 indicate the soil bulk density treatments applied (Mg m^{-3}). Note the different y-axis scales.

708

709 Figure 5. Mean daily N_2O fluxes from soil cores and gas diffusivity (D_p/D_o) over time for
710 the Wakanui soil. The 2 wetting-draining cycles are represented with the first cycle from day
711 0 to 12 and the second from day 13 to 25. The solid black line represents D_p/D_o = 0.006.
712 Numerals in the legend indicate the soil bulk density treatments applied (Mg m^{-3}). Error bars =
713 s.e.m, n=4. The vertical dashed black lines are here to show the days where D_p/D_o = 0.006.

714

715 Figure 6. Mean daily N_2O fluxes from soil cores and gas diffusivity (D_p/D_o) over time for
716 the Otorohanga soil. The 2 wetting-drainage cycles are represented with the first cycle from
717 day 0 to 12 and the second from day 13 to 25. The solid black line represents D_p/D_o = 0.006.
718 Numerals in the legend indicate the soil bulk density treatments applied (Mg m^{-3}). Error bars =
719 s.e.m, n=4. Note D_p/D_o scale is greater than in Figure 7.

720

721 Figure 7. Mean daily N_2O fluxes from soil cores and WFPS over time for the Wakanui
722 soil. The 2 wetting-draining cycles are represented with the first cycle from day 0 to 12 and the
723 second from day 13 to 25. Numerals in the legend indicate the soil bulk density treatments
724 applied (Mg m^{-3}). Error bars = s.e.m, n=4.

725

726 Figure 8. Mean daily N_2O fluxes from soil cores and WFPS over time for the Otorohanga
727 soil. The 2 wetting-draining cycles are represented with the first cycle from day 0 to 12 and the
728 second from day 13 to 25. Numerals in the legend indicate the soil bulk density treatments
729 applied (Mg m^{-3}). Error bars = s.e.m, n=4.

730

731 Figure 9. Mean daily N_2O ^{15}N enrichment (atom %) over time for the Wakanui and the
732 Otorohanga soils. Also shown are the 2 saturation events (vertical dashed lines). Numerals in
733 the legend indicate the soil bulk density treatments applied (Mg m^{-3}). Error bars = s.e.m, n=4.

734

735 Figure 10. Mean daily N_2 fluxes over time for the Wakanui and Otorohanga soils. Also
736 shown are the 2 saturation events (dashed vertical lines). Numerals in the legend indicate the
737 soil bulk density treatments applied (Mg m^{-3}). Error bars = s.e.m, n=4.

738

739

740 Table 1 Soil (0-10 cm) texture, particle density, organic matter and carbon contents. Errors

741 bars are ± standard error of the means; n=6.

	Wakanui		Otorohanga	
	IUSS[a]	USDA[b]	IUSS	USDA
Clay (%)	22.3	22.3	11.3	11.3
Silt (%)	53.4	72.1	39.7	66.6
Sand (%)	24.3	5.6	48.9	22.1
Particle density (g cm^{-3})[c]	2.59 ± 0.01		2.46 ± 0.02	
Soil organic matter (%)[d]	2.70 ± 0.11		3.80± 0.20	
Carbon (%)[d]	1.57 ± 0.06		2.21 ± 0.12	

742 [a]International Union of Soil Science (Clay 0-2 µm, silt 2-20 µm, and sand 20-2000 µm),

743 [b]United States Department of Agriculture (Clay 0-2 µm, silt 2-63 µm, and sand 63-2000 µm)

744 U.K.),

745 [c]Hao et al. (2008),

746 [d]Based on loss on ignition at 500oC (Blakemore et al., 1987).

747

Table 2. Mean soil pH, dissolved organic carbon (DOC), ammonium-N (NH_4^+-N) and nitrate-N (NO_3^--N) concentrations at days 12 and 25, the end of the first and second drainage cycles, respectively. Error bar = s.e.m; n=4 on day 25, n=3 on days 0 and 12.

		Day 0			Day 12			Day 25		
Wakanui	Bulk density (g cm^{-3})	1.0	1.1	1.2	1.0	1.1	1.2	1.0	1.1	1.2
	pH	ND	ND	ND	5.6 ± 0.1	5.6 ± 0.1	5.6 ± 0.2	5.6 ± 0.1	5.7 ± 0.1	5.3 ± 0.1
	DOC (μg C g^{-1} soil)	388 ± 14	460 ±26	402 ± 64	271 ± 5	227 ± 15	250 ± 14	169 ± 6	166 ± 2	147 ± 9
	NO_3^--N (μg NO_3^--N g^{-1} soil)	169 ± 92	170 ± 56	177 ± 95	282 ± 43	262 ± 11	214 ± 53	205 ± 28	216 ± 35	182 ± 18
	NH_4^+-N (μg NH_4-N g^{-1} soil)	48 ± 4	26 ± 8	37 ± 7	70 ± 3	63 ± 5	43 ± 13	1.2 ± 0.2	1.3 ± 0.2	1.6 ± 0.7
Otorohanga	Bulk density (g cm^{-3})	0.9	1.0	1.1	0.9	1.0	1.1	0.9	1.0	1.1
	pH	ND	ND	ND	5.2 ± 0.1	5.2 ± 0.1	5.2 ± 0.1	5.2 ± 0.1	5.2 ± 0.1	5.2 ± 0.1
	DOC (μg C g^{-1} soil)	181 ± 40	141 ±13	152 ± 6	147 ± 12	105 ± 21	149 ± 39	74 ± 5	81 ± 6	79 ± 2
	NO_3^--N (μg NO_3^--N g^{-1} soil)	78 ± 15	175 ± 82	32 ± 24	228 ± 97	178 ± 20	236 ± 43	130 ± 25	166 ± 31	144 ± 15
	NH_4^+-N (μg NH_4-N g^{-1} soil)	3.2 ± 0.4	3.9 ± 0.4	3.6 ± 0.2	9.1 ± 3	11 ± 3	11 ± 3	1.1 ± 0.4	0.7 ± 0.1	2.5 ± 1.6

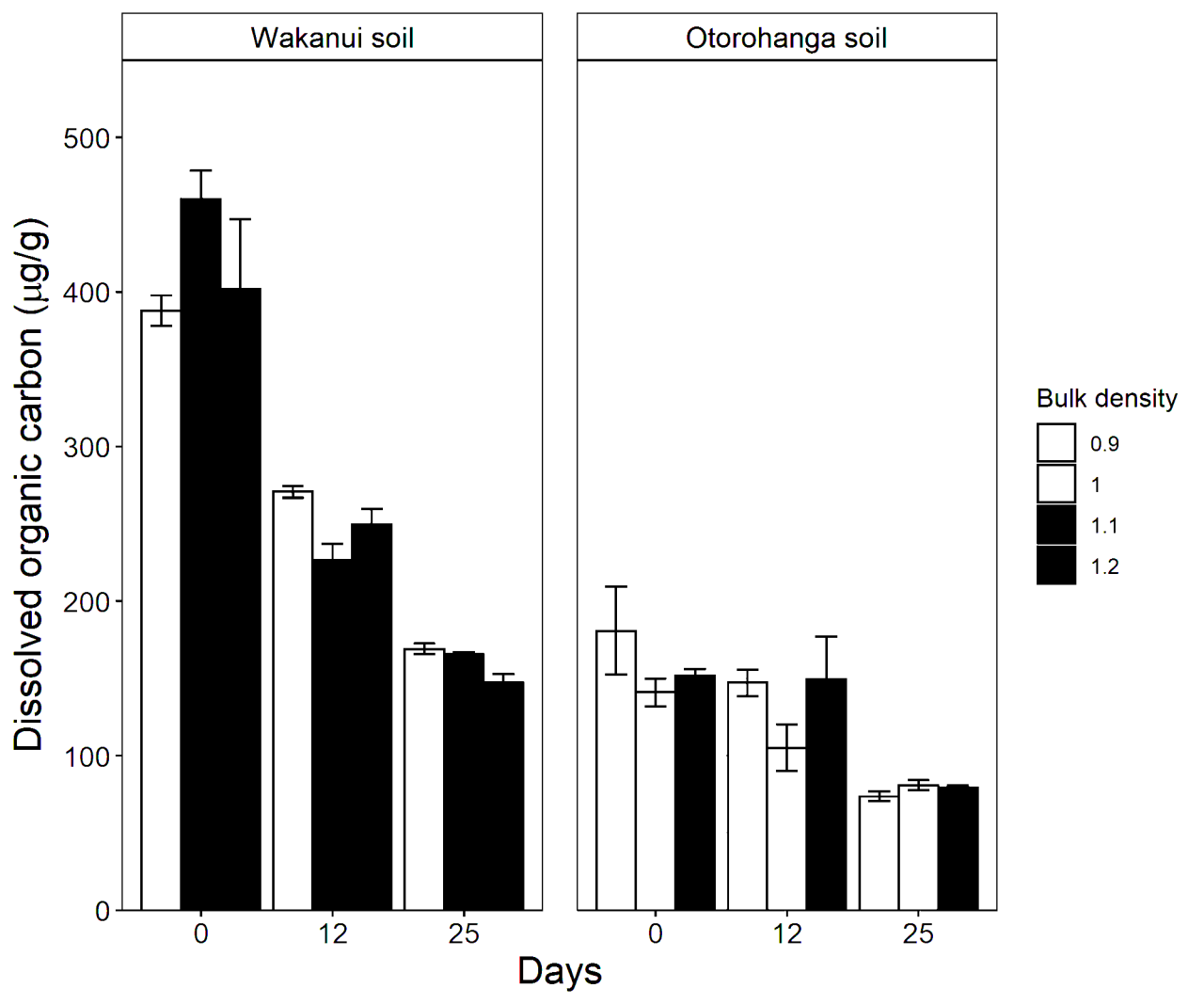
Wakanui soil
Otorohanga soil
Dissolved organic carbon (µg/g)
500
400
300
200
100
0
0
12
25
0
12
25
Days
Bulk density
0.9
1
1.1
1.2

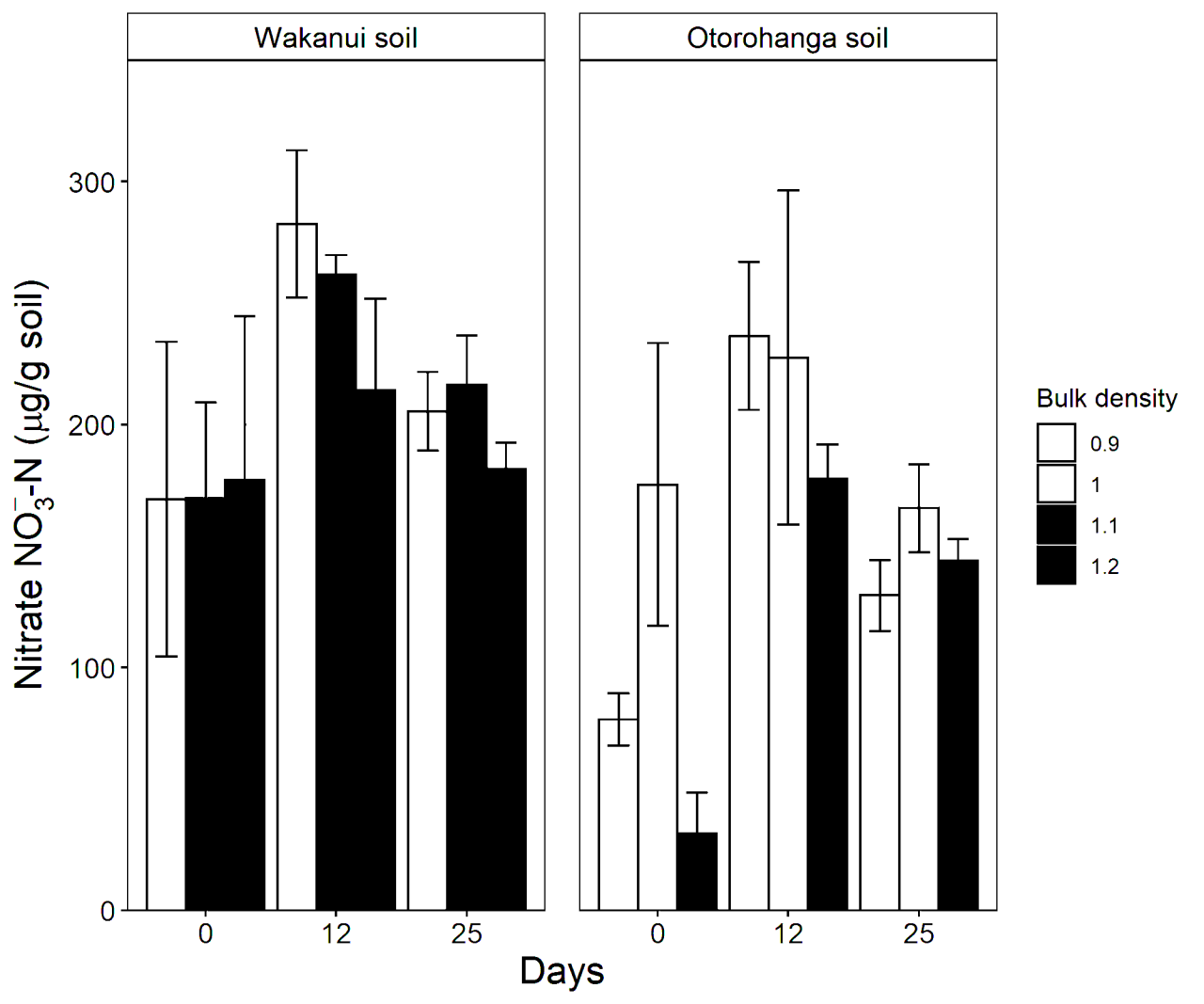
Wakanui soil
Otorohanga soil
Nitrate NO_3^--N (µg/g soil)
300
200
100
0
0
12
25
Days
Bulk density
0.9
1
1.1
1.2

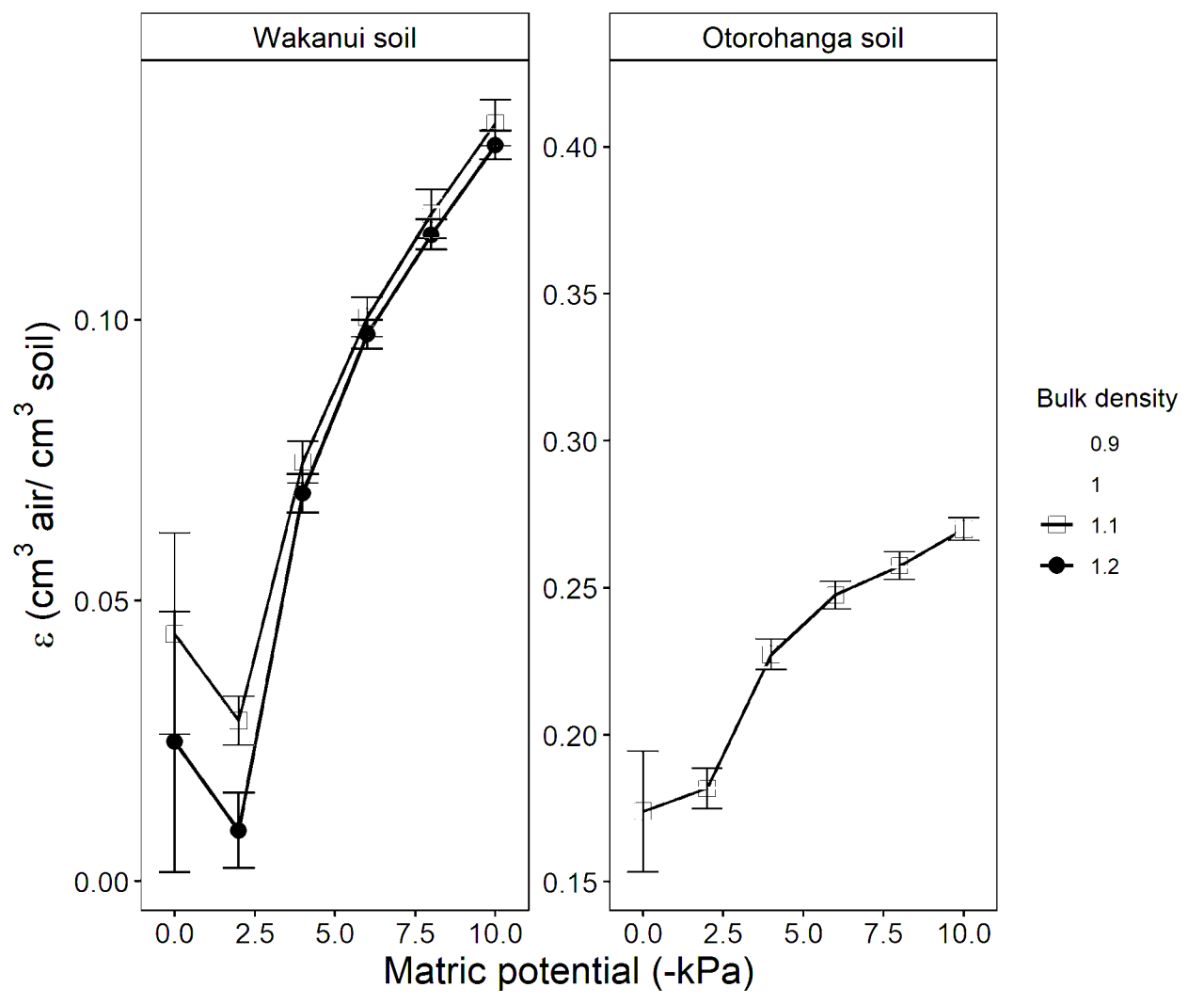
Wakanui soil
Otorohanga soil
ε (cm3 air/ cm3 soil)
0.00
0.05
0.10
0.15
0.20
0.25
0.30
0.35
0.40
0.0
2.5
5.0
7.5
10.0
Matric potential (-kPa)
Bulk density
0.9
1
1.1
1.2

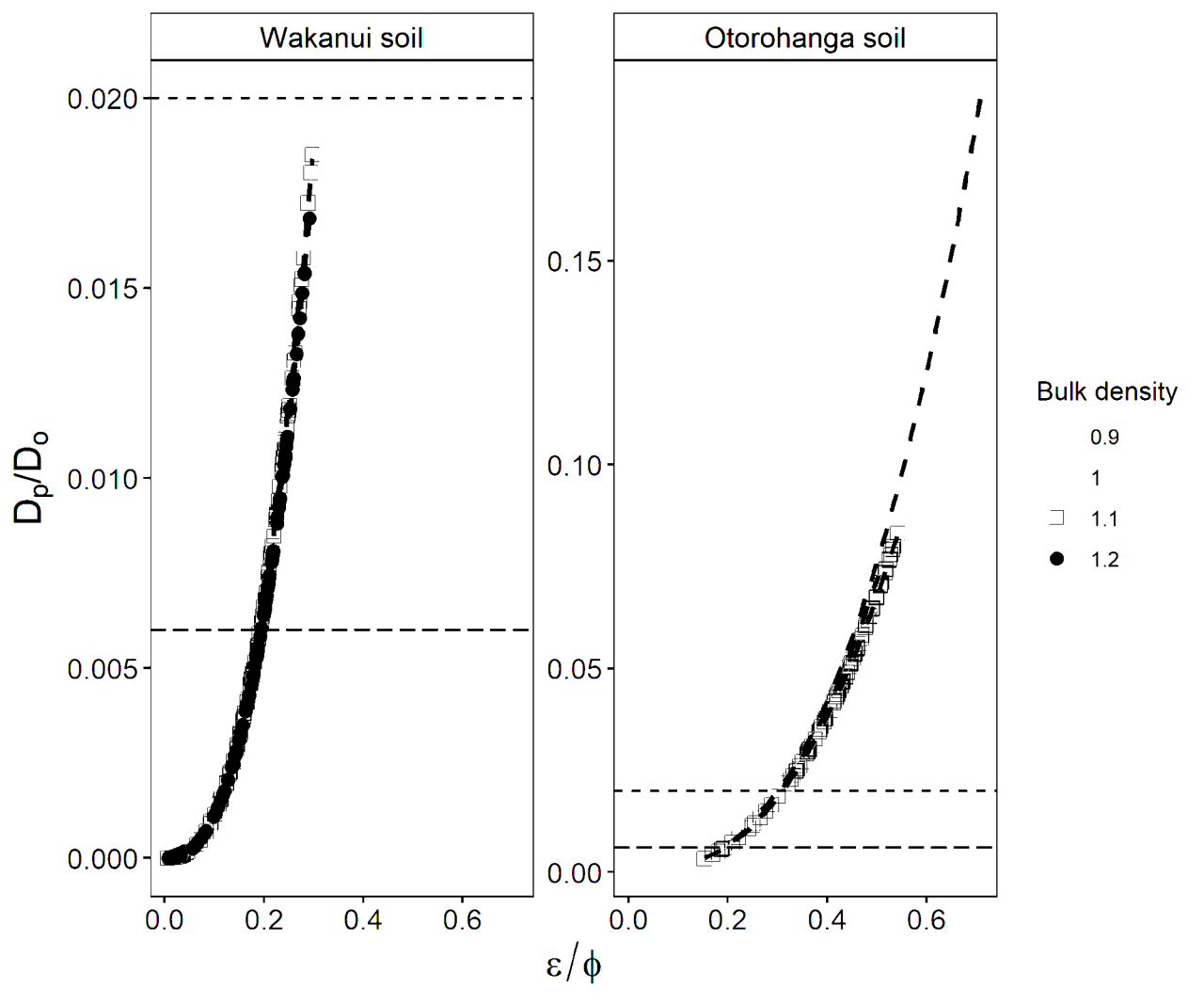
Wakanui soil
Otorohanga soil
D_p/D_o
ε/ϕ
0.020
0.015
0.010
0.005
0.000
0.15
0.10
0.05
0.00
0.0
0.2
0.4
0.6
Bulk density
0.9
1
1.1
1.2

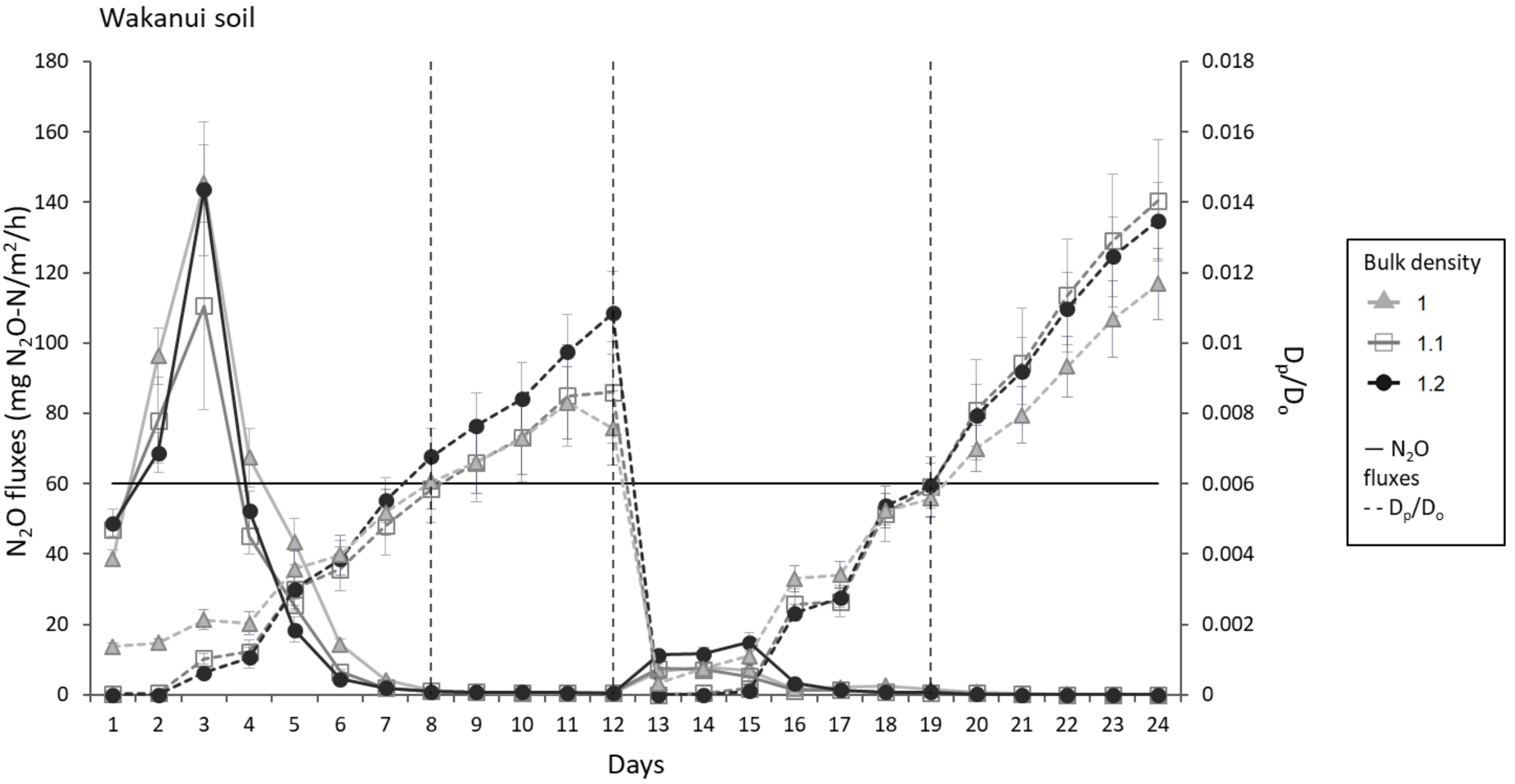
Wakanui soil
N2O fluxes (mg N2O-N/m2/h)
Dp/Do
Days
Bulk density
1
1.1
1.2
N2O fluxes
Dp/Do

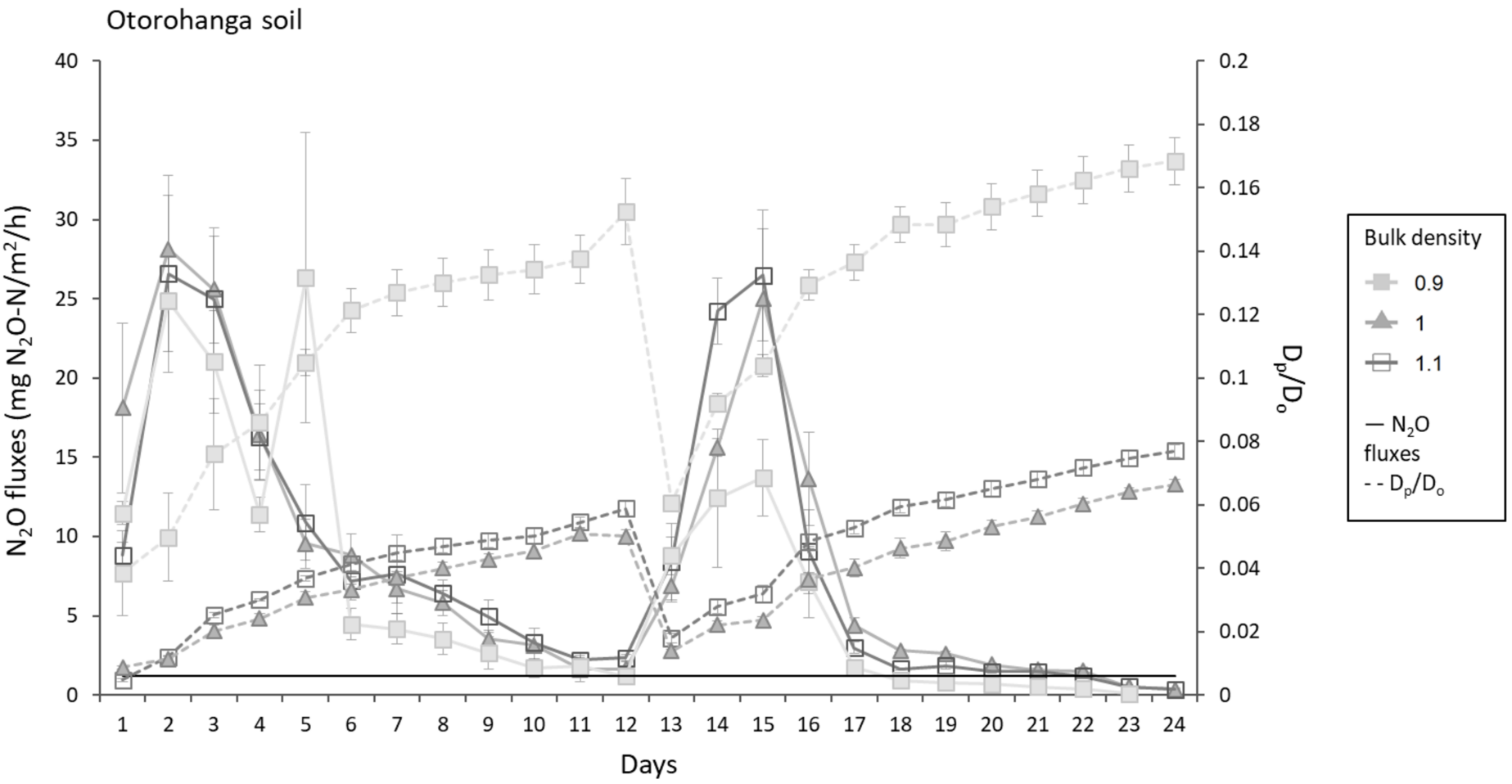
Otorohanga soil
N2O fluxes (mg N2O-N/m2/h)
Dp/Do
Days
Bulk density
0.9
1
1.1
N2O fluxes
Dp/Do

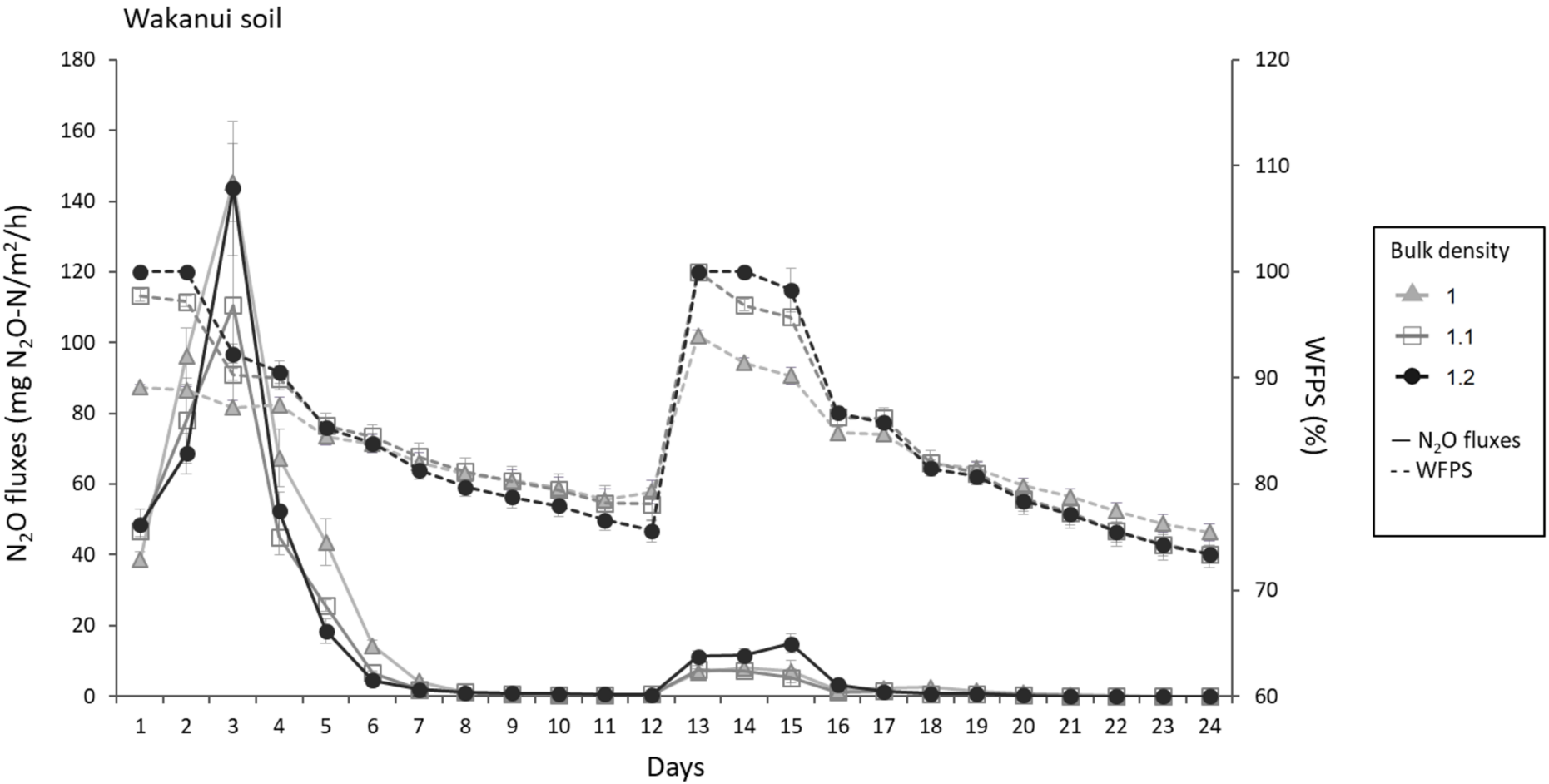
Wakanui soil
N2O fluxes (mg N2O-N/m2/h)
WFPS (%)
Days
Bulk density
1
1.1
1.2
N2O fluxes
WFPS

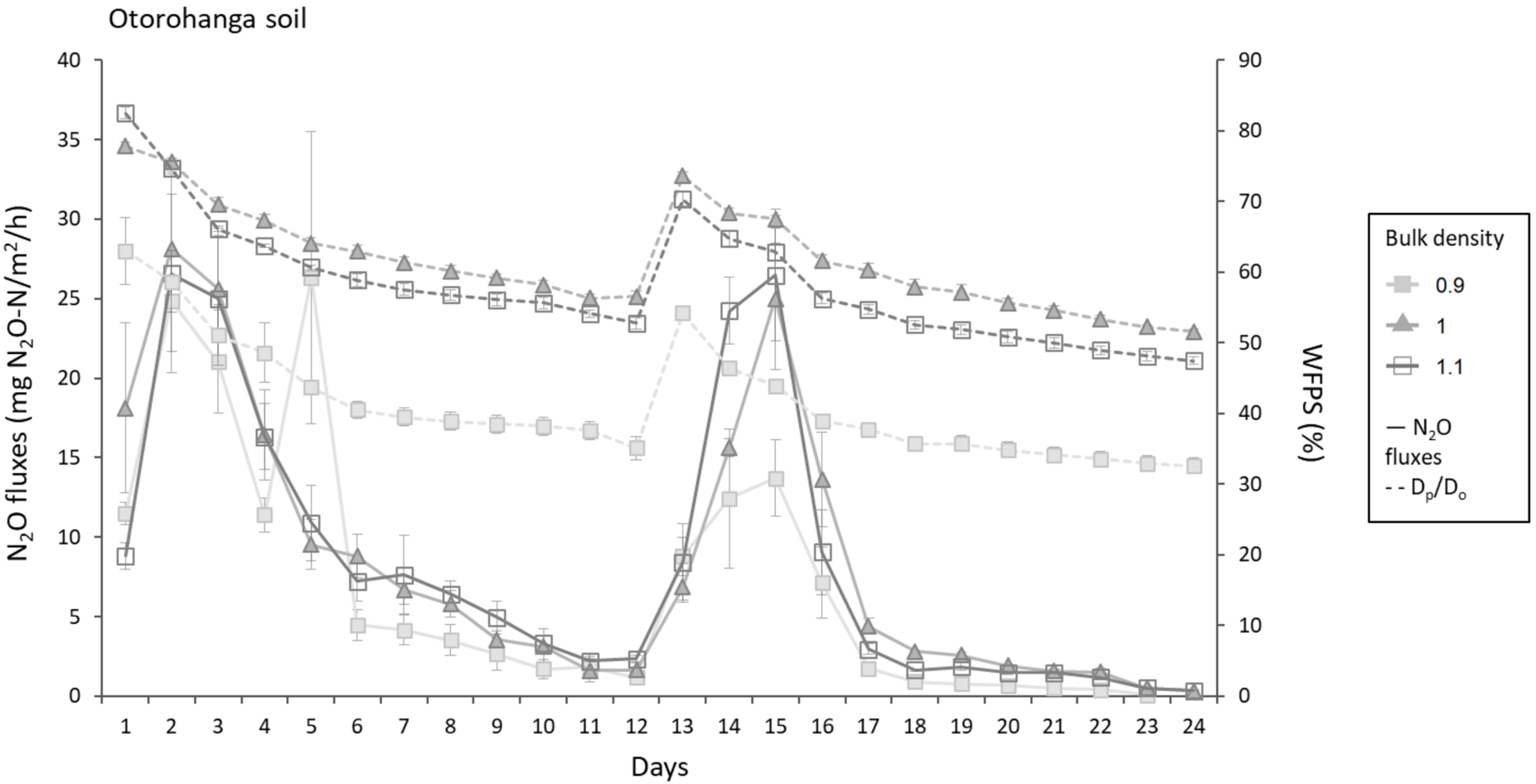
Otorohanga soil
N2O fluxes (mg N2O-N/m2/h)
WFPS (%)
Days
Bulk density
0.9
1
1.1
N2O fluxes
Dp/Do

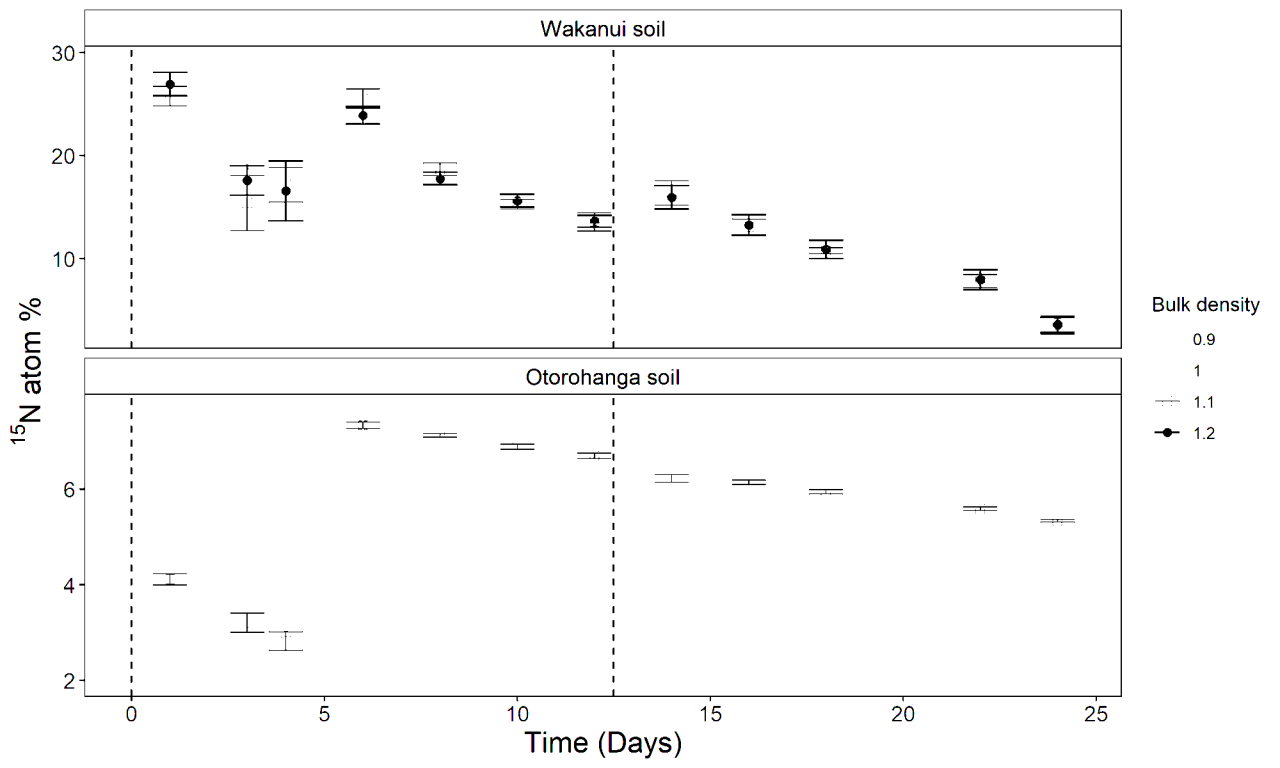
Wakanui soil
Otorohanga soil
30
20
10
6
4
2
0
5
10
15
20
25
^{15}N atom %
Time (Days)
Bulk density
0.9
1
1.1
1.2

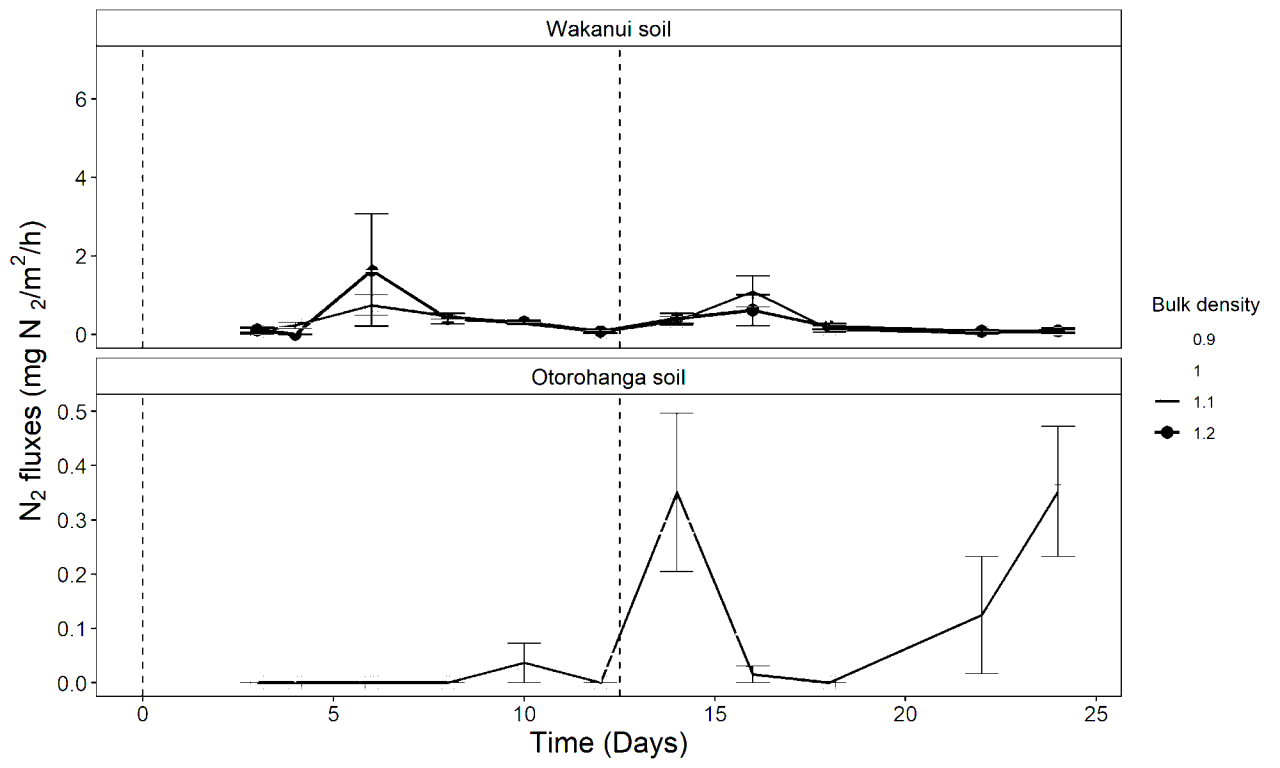
Wakanui soil
Otorohanga soil
N_2 fluxes (mg $N_2/m^2/h$)
Time (Days)
Bulk density
0.9
1
1.1
1.2